ACS APPLIED MATERIALS & INTERFACES

Letter

www.acsami.org

Reversible Structural Transformation and Enhanced Performance of PEDOT:PSS-Based Hybrid Solar Cells Driven by Light Intensity

Joseph Palathinkal Thomas, Saurabh Srivastava, Liyan Zhao, Marwa Abd-Ellah, Donald McGillivray, Jung Soo Kang, Md. Anisur Rahman, Nafiseh Moghimi, Nina F. Heinig, and Kam Tong Leung*

WATLab and Department of Chemistry, University of Waterloo, Waterloo, Ontario N2L3G1, Canada

Supporting Information

ABSTRACT: Hybrid solar cells made of poly(3,4-ethylenedioxythiophene):poly(styrenesulfonate) (PEDOT:PSS) and appropriate amounts of a cosolvent and a fluorosurfactant on planar n-type silicon substrates showed a photoconversion efficiency (PCE) of above 13%. These cells also exhibited stable, reproducible, and high external quantum efficiency (EQE) that was not sensitive to light-bias intensity (LBI). In contrast, solar cells made of pristine PEDOT:PSS showed low PCE and high EQE only under certain measurement conditions. The EQE was found to degrade with increasing LBI. Here we report that the LBI-sensitive variation of EQE of the low-PCE cells is related to a reversible structural transformation from a quinoid to a benzoid structure of PEDOT.

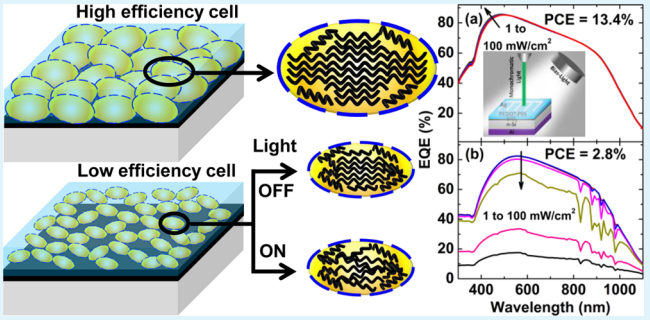

KEYWORDS: *PEDOT:PSS, hybrid solar cell, external quantum efficiency, light-bias intensity, structure stabilization*

Contemporary solar cells comprised of organic or organic−inorganic hybrid materials have attracted a lot of interest in the area of green energy because they offer low-cost fabrication of high-efficiency solar cells.[1−4] Typically, these cells contain a p-type transparent conducting polymer layer, poly(3,4-ethylenedioxythiophene):poly(styrenesulfonate) (PEDOT:PSS), as either an active layer or an electrode.[1−6] Hybrid solar cells made of PEDOT:PSS and n-type silicon substrates have attracted much recent attention because of their simple fabrication processes for low-cost device applications and their high photoconversion efficiencies (PCE) of 10−13%.[3,4,7−17] However, there exists a large discrepancy in the PCE values for these types of solar cells in the literature,[9−17] which is mainly caused by unoptimized PEDOT:PSS properties[12] or interface effects.[14]

The PCE of a solar cell is typically estimated from its current versus voltage ($I-V$) spectrum measured with light illumination under standard one-sun conditions (AM 1.5G, 100 mW/cm^2).[18,19] In addition to $I-V$ data, external quantum efficiency (EQE) measurement has also been used as an important tool to quantify the efficiency of conversion of light to charge carriers as a function of the wavelength of the incident light.[1,2,19−22] The variation of EQE under external light-bias intensity (LBI) in organic solar cells has been discussed in the literature.[2,19−22] More importantly, EQE measurements as a function of LBI have been used to characterize the nature of cell recombination.[19] It is a common belief that the EQE for a good cell should be stable under different LBI conditions. In most solar cell studies reported to date, it is however not a common practice to validate the EQE data against the $I-V$ data. It is therefore not surprising that the EQE performance of the PEDOT:PSS/Si hybrid solar cells under different LBI conditions has yet to be reported. We demonstrate here that EQE measurement under different LBI conditions is an important integral part of ascertaining the robustness of the cell performance because LBI dependence corresponds to an important indicator of underlying structural changes in PEDOT:PSS. Because PEDOT:PSS has been a technologically important conducting polymer, studies of LBI-dependent effects for solar cells made of PEDOT:PSS and silicon could give insight into the structural stability of PEDOT:PSS with different LBIs, which might have important implications in optimizing its properties and further improving the performance of PEDOT:PSS-based electronic devices.

Here, we report that, under no LBI, very high EQE can be obtained for both the high- and low-PCE hybrid solar cells made respectively with and without the addition of ethylene glycol (EG) in PEDOT:PSS. However, the high short-circuit current density estimated from the EQE of the low-PCE cell is contradictory to the value obtained from its $J-V$ data measured under one-sun conditions. Our experiments further reveal a decrease in the EQE with increasing LBI for the low-PCE cells, which is in marked contrast to the extremely stable EQE found for the high-PCE cells. We attribute the latter LBI-insensitive, stable EQE performance of the high-PCE cells to their cosolvent-stabilized quinoid structural changes in PEDOT:PSS.

Received: February 8, 2015
Accepted: April 2, 2015
Published: April 2, 2015

DOI: 10.1021/acsami.5b01252
ACS Appl. Mater. Interfaces 2015, 7, 7466−7470

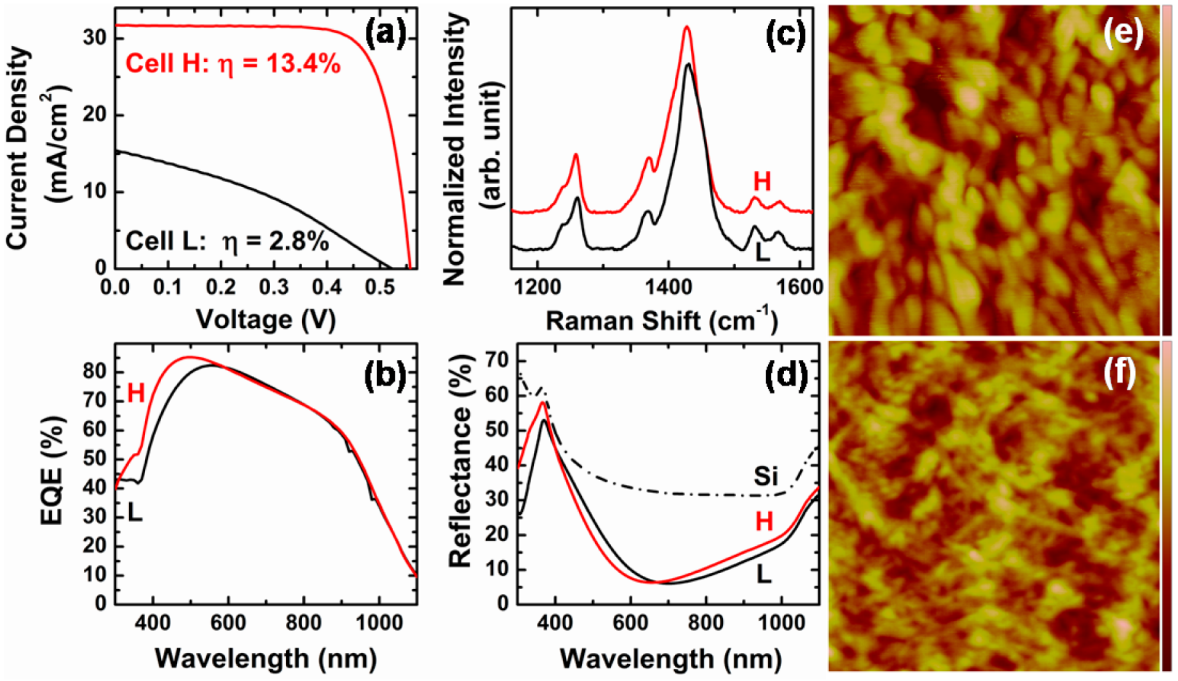

Figure 1. (a) Current density versus voltage, (b) EQE, (c) Raman spectra, and (d) reflectance spectra of high-efficiency (H) and low-efficiency (L) PEDOT:PSS/SiO_x/silicon cells. The high-efficiency cell was made of EG7-PEDOT:PSS, and the low-efficiency cell was made of pristine PEDOT:PSS, both after the addition of 0.25 wt% FS on silicon substrates. AFM images (500 × 500 nm) of (e) high-efficiency and (f) low-efficiency hybrid solar cells with side scale bars of 0−8 nm.

We provide evidence for a relationship between the unstable EQE performances of the low-PCE cells and a reversible structural transformation from a quinoid to a benzoid structure of PEDOT under high-LBI conditions. In addition, the results also suggest that these low-PCE cells are highly efficient for light harvesting in low-light conditions.

The experimental methods are discussed in detail in the Supporting Information (SI). Briefly, PEDOT:PSS (PH1000) was mixed with optimized 7 wt% EG to achieve a highly conducting form.[12] To enhance the wettability of PEDOT:PSS, 0.25 wt% fluorosurfactant (FS) was added. Prior to spin coating of the PEDOT:PSS layer, precleaned n-type silicon substrates were kept in ambient atmosphere for 1.5 h after a hydrofluoric acid dip and bottom aluminum metal electrode deposition. Silver metal deposited in the form of a comb on the PEDOT:PSS layer was used as the top electrode. The solar cell properties (current density, J, vs voltage, V; EQE vs wavelength) of PEDOT:PSS/SiO_x/planar silicon obtained with the addition of 7 wt% EG and 0.25 wt% FS in PEDOT:PSS (hereby designated as EG7-PEDOT:PSS; cell H) and of 0.25 wt% FS added pristine PEDOT:PSS (cell L) are shown in Figure 1. J−V measurement for the cells in the dark shows the standard diode characteristics (Figure S1 in the SI). The main device performance parameters estimated from the J−V curves in Figure 1, including the open-circuit potential (V_{OC}), short-circuit current density (J_{SC}), fill factor (FF), and PCE, are summarized in Table 1. The values in parentheses represent the average values with their standard deviations for the device performance parameters obtained from a set of seven similar cells. The series and shunt resistances of the cells are given in Table S1 in the SI. The highest PCE of 13.4% has been achieved for our best cell made from EG7-PEDOT:PSS (cell H). The average PCE for seven such similar cells is 13.1 ± 0.3%. A low PCE of 2.8% (2.5 ± 0.3%) is obtained for the cell(s) made from pristine PEDOT:PSS (cell L). For both cells H and L, high V_{oc} values are obtained, with 558 (560 ± 5) mV for cell H and 524 (520 ± 7) mV for cell L. Similar to the PCE results, high J_{sc} values of 31.7 (31.1 ± 1.1) mA/cm^2 for cell H and low J_{sc} of 15.5 (14.1 ± 1.4) mA/cm^2 for cell L are obtained. We also obtain high FF values of 76 (71 ± 6) % for the best-performing high-PCE cell. However, a low FF of 34 (32 ± 6) % is found for the low-PCE cell(s). The addition of EG to PEDOT:PSS therefore provides an effective way of improving the PCE performance.

Table 1. Solar Cell Properties of High-Efficiency (Cell H) and Low-Efficiency (Cell L) PEDOT:PSS/SiO_x/Silicon Hybrid Solar Cells[a]

sample	V_{OC} (mV)	J_{SC} (mA/cm^2)	FF (%)	PCE (%)
cell H	558 (560 ± 5)	31.7 (31.1 ± 1.1)	76 (71 ± 6)	13.4 (13.1 ± 0.3)
cell L	524 (520 ± 7)	15.5 (14.1 ± 1.4)	34 (32 ± 6)	2.8 (2.5 ± 0.3)

[a]The values in parentheses correspond to the average values along with their estimated standard deviations obtained from seven similar cells.

The EQE corresponds to the ratio of the number of generated outgoing electrons to the number of photons incident on the device. Our measurements show a maximum EQE (EQE_{max}) of above 85% at 500 nm for cell H and of above 82% at 560 nm for cell L (Figure 1b). The high EQE near the blue-wavelength region suggests a good front surface carrier collection efficiency for cell H,[23,24] which is improved by the addition of EG in PEDOT:PSS. However, the high EQE for cell L (made of pristine PEDOT:PSS) does not correlate with its estimated J_{SC} values from the EQE (~26 mA/cm^2) and J−V data (~15 mA/cm^2). It should be noted that EQE measurement is normally carried out with a light intensity of about 1

DOI: 10.1021/acsami.5b01252
ACS Appl. Mater. Interfaces 2015, 7, 7466−7470

mW/cm^2. To further investigate the apparent inconsistency between the high EQE and low $J-V$ properties of cell L, we have carried out EQE measurements under different LBI conditions, which will be discussed in the latter part of this paper.

Raman spectroscopy can be used to examine the structure of PEDOT, with major Raman peaks for PEDOT observed between 1150 and 1610 cm^{-1}. Figure 1c compares the Raman spectra of PEDOT:PSS for cell H (with EG addition) and cell L (without EG addition). Cosolvent-induced structural transformation in the Raman spectra for the highly conducting form of PEDOT:PSS has already been reported, which is in good accord with our results.[25,26] The features at 1425 and 1453 cm^{-1} correspond to the symmetric stretching modes of quinoid $C_\alpha-C_\beta$ and benzoid $C_\alpha=C_\beta$ components, respectively.[25−28] Peaks at 1530 and 1568 cm^{-1} are attributed to the asymmetric $C_\alpha-C_\beta$ stretching modes. A discernible peak at 1366 cm^{-1} can be assigned to $C_\beta=C_\beta$ stretching vibrations, while the features between 1100 and 1300 cm^{-1} correspond to $C_\alpha=C_{\alpha'}$ stretching modes.[25] It is known that cosolvent addition induces a rearrangement of the PEDOT chains, from the coil-like benzoid structure to a more linear or extended quinoid structure, which increases the size and facilitates closer packing of the PEDOT grains.[12,25,26] The corresponding reflectance spectra of the PEDOT:PSS films on silicon (Figure 1d) show that the PEDOT:PSS layer acts as an antireflection coating on the silicon substrate. For comparison, the reflectance spectrum of the silicon substrate is also included in the figure. A slight blue shift in the reflectance minima for the EG-added sample (cell H) relative to the pristine PEDOT:PSS sample (cell L) is observed, which indicates that the cosolvent addition does not significantly affect the optical properties of these films. This structural rearrangement is also supported by our surface morphological studies. The respective atomic force microscopy (AFM) images show larger ellipsoidal, closely packed grains in EG7-PEDOT:PSS (Figure 1e), in marked contrast to the smaller elongated grains in pristine PEDOT:PSS (Figure 1f). The addition of EG in PEDOT:PSS (cell H) enhances the formation of extended linear quinoid structures, which are believed to give rise to the observed large PEDOT grains.[12]

To determine the origin of low-$J-V$ and high-EQE properties of the cell made of pristine PEDOT:PSS (cell L), EQE measurement is carried out under different LBI conditions. It should be noted that calibration of LBI to match the illumination condition between 1 and 100 mW/cm^2 is difficult because of the complexities in performing such a measurement in situ during EQE measurement. For EQE measurement, the monochromatic beam is incident normal to the sample surface (between the electrodes as shown in the inset in Figure 2a).[20,21] To replicate a LBI similar to that used in $J-V$ measurement, i.e., conducted with LBI normal to the sample surface, is therefore not physically possible. Thus, the LBI is delivered at an angle (approximately 45° from normal) to completely flood the total sample area (Figure 2a, inset). Using a power meter to measure the light intensity, we then adjust the illumination appropriately to reach a maximum intensity of 100 mW/cm^2 (one sun or an appropriately chosen LBI). Figure 2 compares the EQE spectra of cells H and L under different LBI conditions. Evidently, a minute blue shift and an extremely minor increase in the EQE_{max} with increasing LBI are observed for cell H (Figure 2a). In contrast, a significant reduction in the EQE with increasing LBI is found for cell L (Figure 2b). This EQE reduction is particularly

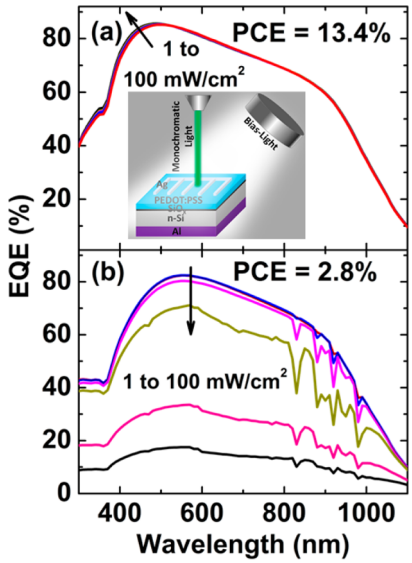

Figure 2. EQE curves under different LBIs (1, 28, 42, 56, 78, and 100 mW/cm^2) of (a) a high-efficiency and (b) a low-efficiency PEDOT:PSS/SiO_x/silicon cells. The inset shows a schematic layout for EQE spectral measurement with the monochromatic light incident normal to the sample surface (between two fingers of the top electrode) and the light bias completely illuminating the entire sample surface at an angle of 45° with respect to the incident monochromatic beam.

apparent with LBI above 40 mW/cm^2. In addition, we observe a series of spectral features between 800 and 1000 nm with increasing LBI, the origin of which is not clear. It is possible that structural changes could produce such changes in the EQE spectrum when exposed to different LBI conditions.

To further investigate the cause of the LBI-induced variation in the EQE found for the low-PCE cell (cell L), we also perform in situ Raman spectroscopy measurement under one-sun LBI conditions (100 mW/cm^2) but do not find any difference in the Raman data. We then subject these cells to one-sun LBI for a prolonged period of time (2 and 5 h) and subsequently measure the Raman spectra (Figure 3a,b). The Raman spectrum of the high-PCE cell (cell H) does not exhibit any changes after exposure to LBI for 2−5 h (Figure 3a). However, the corresponding Raman spectra for the low-PCE cell (cell L) indicate a discernible transformation from a quinoid to a benzoid structure after 2 h of LBI exposure (Figure 3b). The quinoid and benzoid peak positions are marked with vertical lines in the figure. The structural transformation trend becomes more apparent after exposure of cell L to LBI for 5 h.

To summarize these results, we show schematic models of the two cells in Figure 4. For cell H with the EG7-PEDOT:PSS/SiO_x/silicon structure (Figure 4a), EG addition induces the formation of larger PEDOT grains and more orderly compacting of these grains while excess PSS is stabilized at the grain boundaries.[12,29] Such a grain likely consists of linear quinoid chains (Figure 4c). The formation of large grains indicates that EG acts as a boundary layer between PEDOT and PSS chains and helps to extend the linearity of the quinoid structure by converting the coil-like benzoid structures near the grain boundaries. For cell L with a PEDOT:PSS/SiO_x/silicon structure (Figure 4b), smaller grains are arranged more randomly in the film with the coexistence of both linear quinoid and coil-like benzoid structures of PEDOT (Figure 4d). For clarity, we have not depicted micropore defects at the

DOI: 10.1021/acsami.5b01252
ACS Appl. Mater. Interfaces 2015, 7, 7466−7470

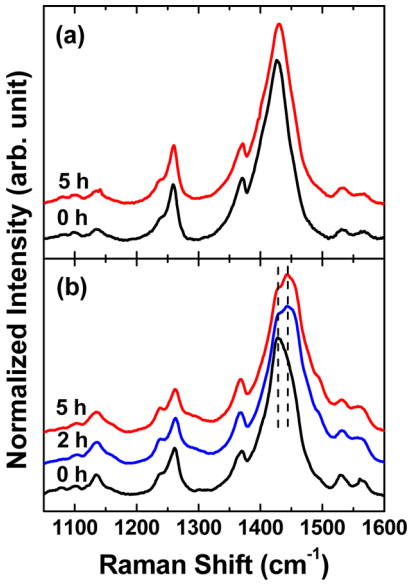

Figure 3. Raman spectra of (a) high-efficiency and (b) low-efficiency PEDOT:PSS/SiO_x/silicon cells before and after continuous light-bias illumination for 0−5 h. The dashed lines in part b mark the changes in the peak positions upon light-bias illumination.

interface between PEDOT:PSS and SiO_x/silicon in these cells, the formation of which has been discussed in our earlier work.[4] The presence of the coil-like benzoid structure could account for the smaller grain size, and their aggregation near the grain boundaries would reduce the charge-transport efficiency. We propose that a high LBI exposure causes considerable structural changes in the PEDOT grains, with reduction in the quinoid chain length and extension of the benzoid chains (Figure 4e). The structural changes are found to be reversible under short LBI exposure, which is confirmed by our observation that high-EQE spectra after exposure of cell L to LBI for a few minutes can be obtained repeatedly. Conversely, the EQE of cell L exposed to LBI for 5 h measured again without LBI (Figure S2 in the SI) indicates a partial structural reversibility. The large EQE variation in organic solar cells subjected to LBI reported in the literature[2,20] may therefore be attributed to reversible structural changes in the PEDOT:PSS layer. Our results do not, however, rule out the earlier suggestions that space-charge buildup[2] and increased recombination are the major causes of the observed EQE variation.[20] It is possible that the structural changes in PEDOT:PSS under LBI exposure could lead to different space-charge generation processes. For pristine PEDOT:PSS (cell L), the structural transformation from quinoid to benzoid limits the hole transport and results in slower charge-carrier dynamics and significant recombination under high LBI. These results indicate that the addition of cosolvent, EG, is beneficial to producing a stable and linear quinoid structure of PEDOT chains, the improved electronic properties of which are better suited for high-performance organic electronic device fabrication. Moreover, the performance of devices made with PEDOT:PSS could be further improved with the introduction of plasmonic nanoparticles or cells made of surface-structured silicon substrates.

In summary, we report highly stable solar cell properties of a high-efficiency PEDOT:PSS/planar silicon hybrid solar cell that is insensitive to light intensity. This is achieved by stabilization of the quinoid structures in PEDOT:PSS with an optimized amount of cosolvent (EG) addition. While LBI-dependent EQE measurement on the low-efficiency cell revealing its high EQE obtained under normal measurement conditions could be misconstrued as a technical problem, LBI-dependent structural changes in pristine PEDOT:PSS are the real culprit to such a phenomenon. Indeed, solar cells made with pristine PEDOT:PSS (without EG) are found to be highly light-intensity-sensitive, which is attributed to the structural switching from quinoid to benzoid in the PEDOT grains. The structural switching increases the charge-carrier concentration and high recombination rate under intense light, which results in the poor performance of these solar cells. These results provide new insight into the positive effect introduced by the addition of an optimized amount of cosolvent in stabilizing the PEDOT structure, which is important to achieving a stable performance from PEDOT:PSS-based organic and organic−inorganic electronic devices.

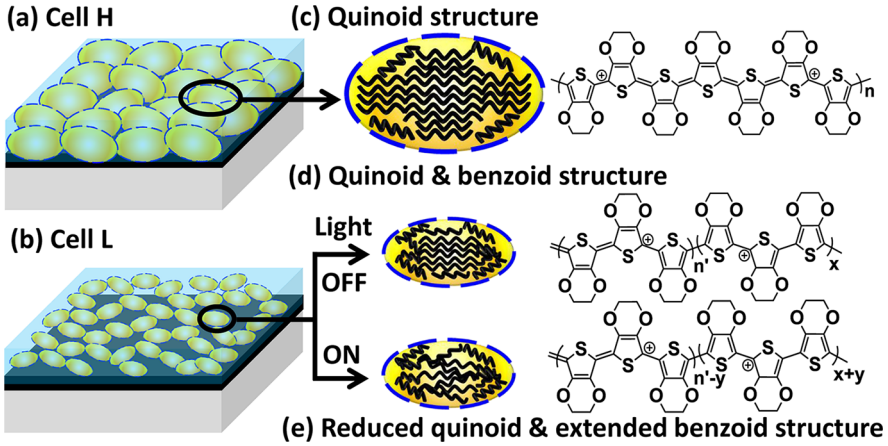

Figure 4. Schematic models of (a) high-efficiency (cell H) and (b) low-efficiency (cell L) cells. Expanded views of a single grain in the respective films with their corresponding chemical structures are shown (c) for cell H with a highly conducting form of the PEDOT quinoid structure after cosolvent addition in PEDOT:PSS, and (d) for cell L with linear quinoid and coil-like benzoid structures present in pristine PEDOT:PSS under no light exposure (OFF) and (e) for structural switching from quinoid to a greater number of benzoid chains under intense light illumination (ON, 100 mW/cm^2).

DOI: 10.1021/acsami.5b01252
ACS Appl. Mater. Interfaces 2015, 7, 7466−7470

■ ASSOCIATED CONTENT

Supporting Information

Additional information and figures as noted in the text. This material is available free of charge via the Internet at http://pubs.acs.org.

■ AUTHOR INFORMATION

Corresponding Author

*E-mail: tong@uwaterloo.ca.

Notes

The authors declare no competing financial interest.

■ ACKNOWLEDGMENTS

This work was supported by the Natural Sciences and Engineering Research Council of Canada. We gratefully acknowledge Dr. Orri Jonsson (PV Measurements, Inc., Boulder, CO) for helpful discussion about EQE measurement under light bias.

■ REFERENCES

(1) Congreve, D. N.; Lee, J.; Thompson, N. J.; Hontz, E.; Yost, S. R.; Reusswig, P. D.; Bahlke, M. E.; Reineke, S.; Voorhis, T. V.; Baldo, M. A. External Quantum Efficiency Above 100% in a Singlet-Exciton-Fission-Based Organic Photovoltaic Cell. *Science* **2013**, *340*, 334−337.

(2) Peumans, P.; Uchida, S.; Forrest, S. R. Efficient Bulk Heterojunction Photovoltaic Cells Using Small-molecular-weight Organic Thin Films. *Nature* **2003**, *425*, 158−162.

(3) Yu, P.; Tsai, C. Y.; Chang, J. K.; Lai, C. C.; Chen, P. H.; Lai, Y. C.; Tsai, P. T.; Li, M. C.; Pan, H. T.; Huang, Y. Y.; Wu, C. I.; Chueh, Y. L.; Chen, S. W.; Du, C. H.; Horng, S. F.; Meng, H. F. 13% Efficiency Hybrid Organic/Silicon-Nanowire Heterojunction Solar Cell via Interface Engineering. *ACS Nano* **2013**, *7*, 10780−10787.

(4) Thomas, J. P.; Leung, K. T. Defect-Minimized PEDOT:PSS/Planar-Si Solar Cell with Very High Efficiency. *Adv. Funct. Mater.* **2014**, *24*, 4978−4985.

(5) Alemu, D.; Wei, H. Y.; Ho, K. C.; Chu, C. W. Highly Conductive PEDOT:PSS Electrode by Simple Film Treatment with Methanol for ITO-Free Polymer Solar Cells. *Energy Environ. Sci.* **2012**, *5*, 9662−9671.

(6) Liu, Q.; Ono, M.; Tang, Z.; Ishikawa, R.; Ueno, K.; Shirai, H. Highly Efficient Crystalline Silicon/Zonyl Fluorosurfactant-Treated Organic Heterojunction Solar Cells. *Appl. Phys. Lett.* **2012**, *100*, 183901.

(7) Wei, W. R.; Tsai, M. L.; Ho, S. T.; Tai, S. H.; Ho, C. R.; Tsai, S. H.; Liu, C. W.; Chung, R. J.; He, J. H. Above-11%-Efficiency Organic−Inorganic Hybrid Solar Cells with Omnidirectional Harvesting Characteristics by Employing Hierarchical Photon-Trapping Structures. *Nano Lett.* **2013**, *13*, 3658−3663.

(8) Chi, D.; Qi, B.; Wang, J.; Qu, S.; Wang, Z. High-performance Hybrid Organic−Inorganic Solar Cell Based on Planar n-type Silicon. *Appl. Phys. Lett.* **2014**, *104*, 193903.

(9) Jeong, S.; Garnett, E. C.; Wang, S.; Yu, Z.; Fan, S.; Brongersma, M. L.; McGehee, M. D.; Cui, Y. Hybrid Silicon Nanocone−Polymer Solar Cells. *Nano Lett.* **2012**, *12*, 2971−2976.

(10) Nagamatsu, K. A.; Avasthi, S.; Jhaveri, J.; Sturm, J. C. A 12% Efficient Silicon/PEDOT:PSS Heterojunction Solar Cell Fabricated at < 100 °C. *IEEE J. Photovolt.* **2014**, *4*, 260−264.

(11) He, L.; Jiang, C.; Wang, H.; Lai, D.; Rusli. Si Nanowires Organic Semiconductor Hybrid Heterojunction Solar Cells Toward 10% Efficiency. *ACS Appl. Mater. Interfaces* **2012**, *4*, 1704−1708.

(12) Thomas, J. P.; Zhao, L.; McGillivray, D.; Leung, K. T. High-efficiency Hybrid Solar Cells by Nanostructural Modification in PEDOT:PSS with Co-solvent Addition. *J. Mater. Chem. A* **2014**, *2*, 2383.

(13) Shiu, S. C.; Chao, J. J.; Hung, S. C.; Yeh, C. L.; Lin, C. F. Morphology Dependence of Silicon Nanowire/Poly(3,4-ethylenedioxythiophene):Poly(styrenesulfonate) Heterojunction Solar Cells. *Chem. Mater.* **2010**, *22*, 3108−3113.

(14) Thomas, J. P.; Zhao, L.; Abd Ellah, M.; Heinig, N. F.; Leung, K. T. Interfacial Micropore Defect Formation in PEDOT:PSS-Si Hybrid Solar Cells Probed by TOF-SIMS 3D Chemical Imaging. *Anal. Chem.* **2013**, *85*, 6840−6845.

(15) Pudasini, P. R.; Ruiz-Zepeda, F.; Sharma, M.; Elam, D.; Ponce, A.; Ayon, A. A. High Efficiency Hybrid Silicon Nanopillar−Polymer Solar Cells. *ACS Appl. Mater. Interfaces* **2013**, *5*, 9620−9627.

(16) Sharma, M.; Pudasini, P. R.; Ruiz-Zepeda, F.; Elam, D.; Ayon, A. A. Ultrathin, Flexible Organic−Inorganic Hybrid Solar Cells Based on Silicon Nanowires and PEDOT:PSS. *ACS Appl. Mater. Interfaces* **2014**, *6*, 4356−4363.

(17) Pudasini, P. R.; Sharma, M.; Ruiz-Zepeda, F.; Ayon, A. A. Efficiency Improvement of a Nanostructured Polymer Solar Cell Employing Atomic Layer Deposited Al_2O_3 as a Passivation Layer. *Microelectron. Eng.* **2014**, *119*, 6−10.

(18) Shockley, W.; Queisser, H. J. Detailed Balance Limit of Efficiency of p−n Junction Solar Cells. *J. Appl. Phys.* **1961**, *32*, 510−519.

(19) Shrotriya, V.; Li, G.; Yao, Y.; Moriarty, T.; Emery, K.; Yang, Y. Accurate Measurement and Characterization of Organic Solar Cells. *Adv. Funct. Mater.* **2006**, *16*, 2016−2023.

(20) Brenner, T. J. K.; Vaynzof, Y.; Li, Z.; Kabra, D.; Friend, R. H.; McNeill, C. R. White-Light Bias External Quantum Efficiency Measurements of Standard and Inverted P3HT:PCBM Photovoltaic Cells. *J. Phys. D: Appl. Phys.* **2012**, *45*, 415101.

(21) Brenner, T. J. K.; Li, Z.; McNeill, C. R. Phase-Dependent Photocurrent Generation in Polymer/Fullerene Bulk Heterojunction Solar Cells. *J. Phys. Chem. C* **2011**, *115*, 22075−22083.

(22) Brenner, T. J. K.; Hwang, I.; Greenham, N. C.; McNeill, C. R. Device Physics of Inverted All-polymer Solar Cells. *J. Appl. Phys.* **2010**, *107*, 114501.

(23) Shen, X.; Sun, B.; Liu, D.; Lee, S. T. Hybrid Heterojunction Solar Cell Based on Organic-Inorganic Silicon Nanowire Array Architecture. *J. Am. Chem. Soc.* **2011**, *133*, 19408−19415.

(24) Holman, Z. C.; Descoeudres, A.; Barraud, L.; Fernandez, F. Z.; Seif, J. P.; Wolf, D. S.; Ballif, C. Current Losses at the Front of Silicon Heterojunction Solar Cells. *IEEE J. Photovolt.* **2012**, *2*, 7−15.

(25) Ouyang, J.; Xu, Q.; Chu, C. W.; Yang, Y.; Li, G.; Shinar, J. On the Mechanism of Conductivity Enhancement in Poly(3,4-ethylenedioxythiophene):Poly(styrene sulfonate) Film Through Solvent Treatment. *Polymer* **2004**, *45*, 8443−8450.

(26) Lapkowski, M.; Pron, A. Electrochemical Oxidation of Poly(3,4-ethylenedioxythiophene)—"in situ" Conductivity and Spectroscopic Investigations. *Synth. Met.* **2000**, *110*, 79−83.

(27) Garreau, S.; Louarn, G.; Buisson, J. P.; Froyer, G.; Lefrant, S. In Situ Spectroelectrochemical Raman Studies of Poly(3,4-ethylenedioxythiophene) (PEDT). *Macromolecules* **1999**, *32*, 6807−6812.

(28) Mukherjee, S.; Singh, R.; Gopinathan, S.; Murugan, S.; Gawali, S.; Saha, B.; Biswas, J.; Lodha, S.; Kumar, A. Solution-Processed Poly(3,4-ethylenedioxythiophene) Thin Films as Transparent Conductors: Effect of *p*-Toluenesulfonic Acid in Dimethyl Sulfoxide. *ACS Appl. Mater. Interfaces* **2014**, *6*, 17792−17803.

(29) Kim, N.; Lee, B. H.; Choi, D.; Kim, G.; Kim, H.; Kim, J. R.; Lee, J.; Kahng, Y. H.; Lee, K. Role of Interchain Coupling in the Metallic State of Conducting Polymers. *Phys. Rev. Lett.* **2012**, *109*, 106405.

DOI: 10.1021/acsami.5b01252
ACS Appl. Mater. Interfaces 2015, 7, 7466−7470